European Geothermal Congress 2013
Pisa, Italy, 3-7 June 2013

Multi-offset VSP for the integrated geophysical characterization of the Grado (NE Italy) carbonatic reservoir

Flavio Poletto[1], Piero Corubolo[1], Biancamaria Farina[1], Andrea Schleifer[1], Lorenzo Petronio[1] and Bruno Della Vedova[2]

[1] OGS (Istituto Nazionale di Oceanografia e di Geofisica Sperimentale)
Borgo Grotta Gigante 42/c, Sgonico (Trieste) Italy

[2] Dept. of Engineering and Architecture, Trieste University
Via Valerio, 10, I-34127 Trieste, Italy

email fpoletto@ogs.trieste.it

Keywords: geothermal exploration, borehole seismic, carbonatic reservoir

ABSTRACT

We present the results of a multi-offset vertical seismic profile (VSP) acquired in a geothermal exploration well in the framework of an integrated VSP, seismic and gravimetric survey. The purpose of the VSP survey was to link borehole logs and seismic data, and to calibrate the surface seismic data acquired for imaging purposes in the area surrounding the well. The VSP allowed us to obtain high-resolution seismic information in depth, and to measure the variations of the physical rock properties in the fractured carbonatic formations at lateral positions, by means of multi-offset data processing and wavefield analysis including anisotropy and Vp/Vs ratio. The VSP provided additional and robust geophysical information for the numerical estimation of the fluid-dynamic modelling of the geothermal-doublet system. The results have been subsequently used for the location of the second well that will be drilled in the geothermal reservoir.

1. INTRODUCTION

In the framework of the integrated seismic and gravity geophysical survey recently conducted in and around Grado (NE Italy) downtown (Petronio et al., 2012; Della Vedova et al., 2013), a multi-offset vertical seismic profile (VSP) was performed in the first exploration well (Grado-1) drilled in 2008 in the geothermal reservoir.

The aim of the integrated geophysical study was to improve the knowledge of the faulted area around the Grado-1 well, to provide data useful to estimate the location and extent of the fractured system, with the target to locate the second well of the geothermal system developed for district heating. In this context, the purpose of the VSP survey was to link borehole and surface seismic data, to calibrate the new surface seismic data acquired for imaging purposes in the area surrounding the well, to obtain high-resolution seismic information in depth, and in general to measure the variations of the physical rock properties in the fractured carbonatic formations encountered below 616,5 m depth at the well location. The borehole integrated approach provides additional and robust geophysical information for the numerical estimation of the fluid-dynamic modelling of the geothermal-doublet system, for reducing the drilling risk of the second well and for evaluating the optimal conditions for the sustainability of the geothermal system.

2. SURVEY DESCRIPTION

The multi-offset survey consists of four offset VSPs, measured at increasing distances from well head using different acquisition parameters. The total investigated depth is 1100 m in the borehole, completed with a cased section down to 696 m depth, the remaining well section down to total depth being open hole. This deeper part is well characterized by drilling measurements, three cores and conventional logs, acoustic and formation, neutron, porosity, gamma ray, and density logs, including a circumferential borehole imaging log (CBIL) providing detailed images of the fractures encountered by drilling, distributed with different patterns and orientation in the carbonatic formations (Cimolino et al., 2010).

At a distance of 44 m from wellhead, a near-offset VSP was measured with high-resolution parameters, using 5 m of depth sampling interval to characterize in detail the vertical seismic profile along the well. Then three offset VSP were acquired at increasing distances. The offset VSPs were aimed at investigating the lateral structural features. The second, third and fourth vertical profiles were acquired with larger depth intervals, of 10, 10 and 20 m, respectively. The second offset (266 m) and third (449 m) offset VSPs were planned after evaluating the surface seismic data and the results of the near-offset VSP. The last VSP was acquired at a large offset of 939 m, with the purpose of investigating the signal propagation in a complex fractured zone interpreted at lateral side position with respect to the well. Due also to logistic conditions in the Grado island, all the VSPs were acquired only by an in-line disposition of the source (accelerated drop-

ping weight, Hydrapulse) points, along the direction of one of the lines (line G13) of the surface reflection seismic survey crossing the exploration well and heading to the East.

3. NEAR OFFSET VSP

The borehole seismic results obtained by the near-offset survey fill the scale gap between the well data and the surface reflection seismic data.

3.1 Near-well formation characterization

The VSP provides the link to the high-resolution well logs and to the data of the borehole lithological profile, and improves the detection and the interpretation of the transition within the carbonatic formation recognized by the lower-resolution surface reflection seismic.

Figure 1 shows the two-way-time (TWT) deconvolved upgoing signals after wavefield separation compared to the log profiles. Signals have good quality and resolution, with frequency bandwidth extended up to 200 Hz. The arrows indicate the correspondence of the interpreted reflections compared with the main lithological changes and the image of the fractures in the borehole imaging log. Important changes indicated by blue arrows are related to the transition from Neogene sediments to the top of the Paleogene carbonate platform at 616.5 m depth, the top of the geothermal reservoir, and the transition to the Mesozoic carbonates at 1007 m depth. The carbonatic depth section is characterized by important sloping fractures indicated by red arrows and encountered by drilling, in the zone immediately below the casing shoe, and, with different patterns of densely distributed fractures, in the deeper zone of the carbonate reservoir after 990 m depth.

Figure 2 shows the vertical interval-velocity profile measured by the near offset VSP, which evidences the velocity changes for compressional waves relative to the interpreted zones, in particular the sudden increase in the velocity at about 610 m depth where the top of the carbonate platform is encountered.

Figure 3 shows the link provided by the near-offset VSP between the formation changes interpreted in depth and the time section of the surface seismic survey passing through the well (see Della Vedova et al., 2013). Figure 3a is the TWT up-going VSP where the transitions to and in the limestone platform are at depths indicated by continuous vertical lines, and the corresponding times are indicated by dashed horizontal lines. Figure 3b represents the TWT VSP, transposed and compared to a portion of the surface seismic section (c). The interpreted formation changes are clearly identified in the seismic section with the support of the VSP signal. The information of the near-offset VSP is used for subsequent depth conversion of the surface seismic data, by time-to-depth model calibration and migration to get imaging and structural information at side well position. This result is improved by robust multi-offset data analysis.

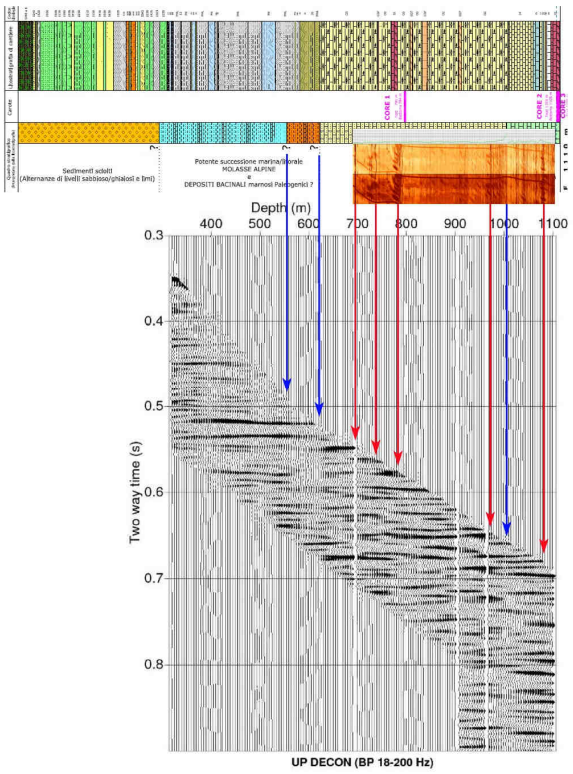

Figure 1: Near offset VSP, Z component, TWT up-going reflection signal. Comparison between CBIL log, stratigraphic profile and VSP. The correspondences between lithological changes, fractured zones and VSP signal are shown.

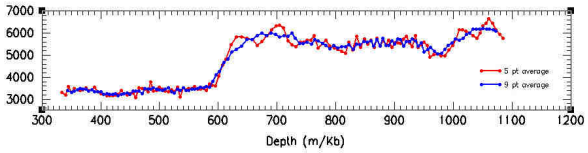

Figure 2: Velocity function calculated by first break picking of near-offset VSP, averaged on 5 (red line) and 9 (blue line) points.

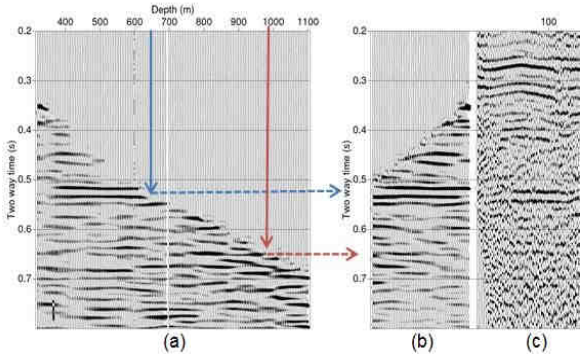

Figure 3: Correspondence between TWT near-offset VSP (a), transposed VSP (b), and a portion of the surface seismic line G13 passing through the well (c).

3.2 Attenuation analysis

Quality factor analysis indicates different attenuation zones between shallow and deep carbonatic formations. The borehole velocity profiles were used to tune the time to depth conversion in the surface seismic imaging, showing the tectonic fabric of the main structural changes. We used two approaches to estimate attenuation in the borehole formation. The first is based on the spectral ratio method, which calculates the cumulative attenuation B_z between different depth intervals (Hauge, 1981) by

$$\left[\ln\frac{A_z(f)}{A_0(f)}\right] = -B_z f + \ln G_z, \quad [1]$$

where A_z is the amplitude spectrum at depth z, G is a frequency-independent geometric factor, and f is the frequency, and using the modified exponential approach proposed by Blias (2012). Figure 4 shows the cumulative attenuation profile obtained by the analysis of the separated downgoing signals of the near-offset VSP. Higher attenuation with lower Q factor of the order of 20 was observed in the shallower alluvium zone, while lower attenuation with Q factor of the order of 200 characterizes the carbonatic formation at 0.55 s in the two-way-time (TWT) section, with some variations in the deeper borehole zone, at 0.65 s (lower carbonate platform) in the time section.

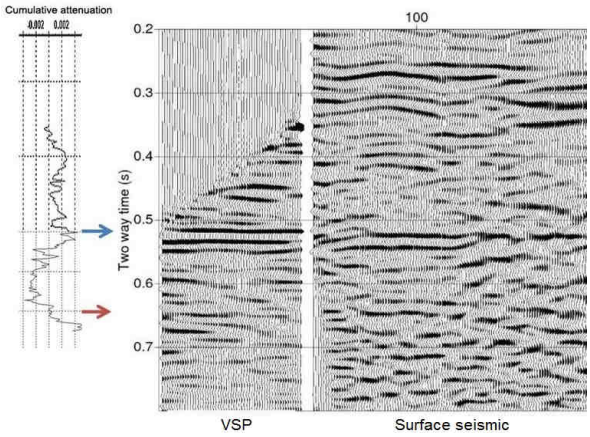

Figure 4: Example of cumulative attenuation analysis by spectral-ratio method, and reflection signal interpretation.

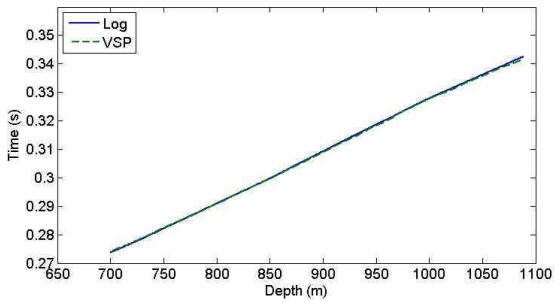

Figure 5: Example of attenuation analysis by comparison of log and VSP arrival times after dispersion compensation.

This result is confirmed by the second approach using the available acoustic log and accurate measured travel-times in the near-offset VSP. The Kramers-Krönig relationship linking the velocity dispersion and the attenuation for physical signals can be approximated as (Sun, Milkereit and Schmitt, 2009)

$$\frac{V(f_2)}{V(f_1)} = 1 + \frac{1}{\pi Q}\ln\left(\frac{f_2}{f_1}\right) \quad [2]$$

where V is the formation velocity, f_1 is the VSP frequency and f_2 the log frequency. Figure 5 shows the good agreement between the VSP travel-time curve and the log integrated-time curve compensated by Eq. [2] assuming Q = 200 for the correction of the dispersion in the limestone section.

4. MULTI-OFFSET VSP PROCESSING

4.1 Multi-offset VSP

Together with lateral seismic imaging, the analysis of the full waveform offset signals and of the viscoelastic synthetic signals (including anisotropy) improved the characterization of the reservoir model coherent with the available geological and geophysical data. The results include the recognition of changes in the elastic rock properties within the reservoir formations obtained using the converted components to estimate the Vp/Vs ratio.

4.2 Signal analysis

Multi-offset data picking provided lateral information to determine the velocity variation at lateral side positions along the seismic line G13 (Petronio et al. 2012; Della Vedova et al., 2013). We used multi-component full waveform data before wavefield separation to improve geological model information. In the preliminary processing phase, the VSP data were rotated with angles calculated in a signal time window around compressional direct arrivals, to obtain the radial R and the vertical-transverse T components starting from the recorded vertical and horizontal ones (Z, H_1 and H_2). In this process, the horizontal components measured with variable orientation at depth are rotated in the direction of maximum energy.

Then the maximum H and the Z components are rotated, assuming that lateral effects are negligible (this is also verified by surface seismic), to get the radial R and transverse T signals for the VSP recorded at 266, 449 and 939 m offset. Figure 6 shows the radial components of the VSP at offset 266 and 449 m.

The full-waveform real data, total field before wavefield separation, were compared to numerical modelling results. Numerical synthetic signals (Z and H components) were calculated using a 2D visco-elastic finite-difference (FD) code. The vertical source is a Ricker wavelet with 30 Hz peak frequency, and the signal propagation is calculated for 2 s, with the output time sampling rate of 1 ms.

4.3 Anisotropy

Vertical-transverse-isotropy (VTI) was assumed for the model, to account for velocity variations in the overburden composed of loose sediments (sand/clay) and basinal marly sediments. The anisotropy parameter was tuned by analysis of direct signals in the real and synthetic offset data, by minimizing the error energy as described in the next paragraph. Anisotropy was estimated and added to the model in the depth range 390 - 600 m using the $\epsilon = 0.1$ as Thomsen's parameter (Thomsen, 1986).

4.4 Analysis by direct arrivals

The gather of the multi-offset VSP provides a set of sparse traces in offset. We analysed them to tune the geological model. The analysis of the direct arrivals was done using the Z, R and T components obtained after signal orientation (Fig. 6 shows an example of radial traces). The signals of the corresponding synthetic model were also rotated in the radial and transverse directions. The real signal was interpreted and compared to the result of the synthetic model, which was tuned to obtain the minimization of the error energy in the measured (picked) travel times at corresponding offsets and depths. Figure 7 shows the result of the travel time comparison for the near offset and for all the offset VSPs. The analysis, including anisotropy and attenuation in the calculation of the synthetic data, allowed us to calibrate local velocity, interpreting and picking corresponding signals, and to tune the model at depth using the large-offset data to estimate a velocity variation at lateral distance from the well of approximately 500 m in the carbonatic layers (Fig. 8).

4.5 Analysis by converted waves

The rotated signals were also used to interpret the converted components, and to estimate local shear-velocity variations. The analysis shows that the observed data – as it can be expected for a fractured formation filled by fluids – can not be explained by the assumption of a Poisson medium (Eberhart-Philips et al., 1995). Figures 9 and 10 show different offset VSP components and the corresponding synthetic signals. The transmitted converted PS waves are clearly interpretable in the transverse components (the T components calculated using the direct arrival). The travel time comparison is shown in Fig. 11, for the offset VSPs. Assuming a Poisson's medium, we see large differences between the real and the synthetic calculated times (left bottom). We modeled and analysed these signals to determine the Vp/Vs ratio, taking into account the variation in the transmitted PP and PS travel paths as shown in Figs. 12 and 13. This provides Vp/Vs information useful to characterize the local rock properties and assess the presence of fluids and fractures associated to higher Vp/Vs ratio (Eberhart-Philips et al., 1995) in the proximity of the borehole, while the analysis of only the P direct arrivals provides information at larger distances from the well, as shown in the previous section.

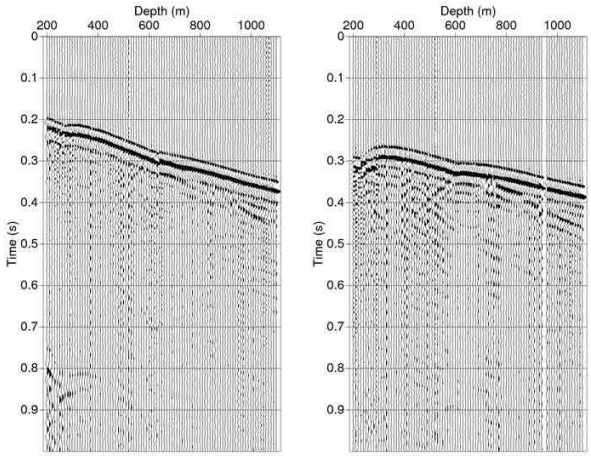

Figure 6: Radial signals of the VSPs at 266 m (left panel) and 449 m (right panel) offset.

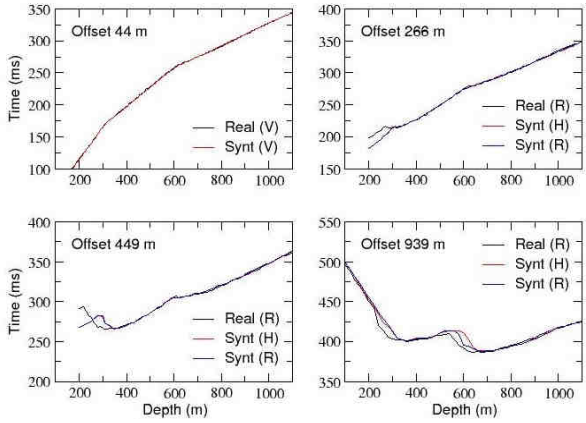

Figure 7: Analysis of direct-arrival travel times in synthetic and real data for the four VSP of the survey. From left top to right bottom: curves of the near offset, 266 m, 449 m and 939 m offset VSP. Matching of the curves is good for all the offsets.

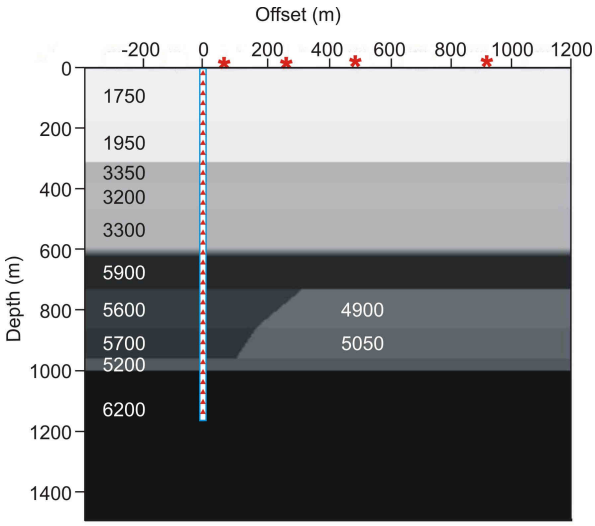

Figure 8: Model estimated by error-energy minimization of the offset VSP travel times of Fig. 7.

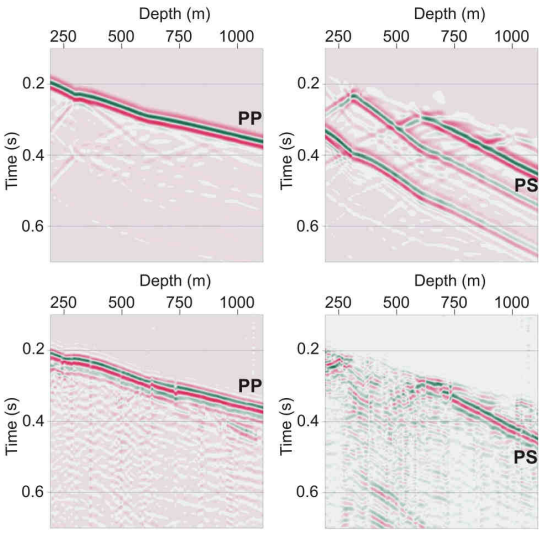

Figure 9: VSP at 266 m offset. On the left: real (top) and synthetic (bottom) radial R signals. On the right: real (top) and synthetic (bottom) transverse T signals.

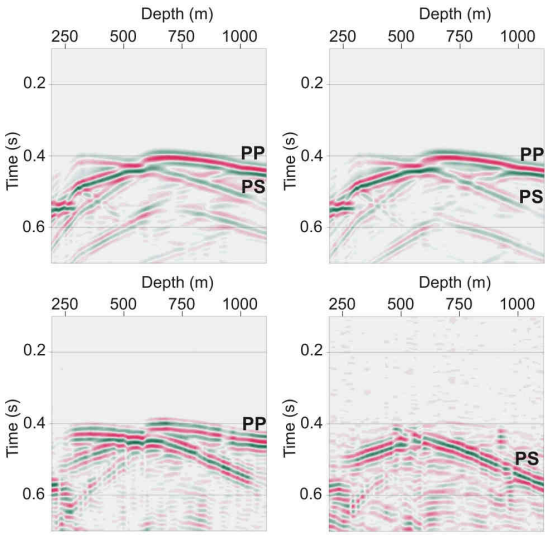

Figure 10: VSP at 939 m offset. Synthetic H direct and converted waves calculated with Poisson (top left) and higher Vp/Vs ratio (top right), and real (bottom) rotated R and T signals.

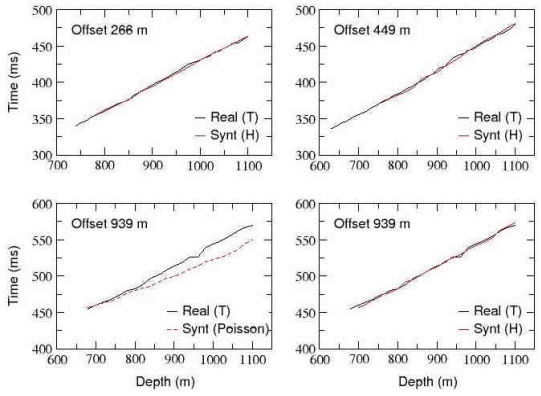

Figure 11: Comparison of real and synthetic arrival times for converted waves using a Poisson medium (left bottom) and after tuning Vp/Vs.

4.6 Imaging

The offset VSP data have been processed to obtain a multi-offset section and reflection imaging. For this purpose the rotated up- and down-going wavefields were separated, and deconvolved. We used the transverse component to obtain images of the reflection section.

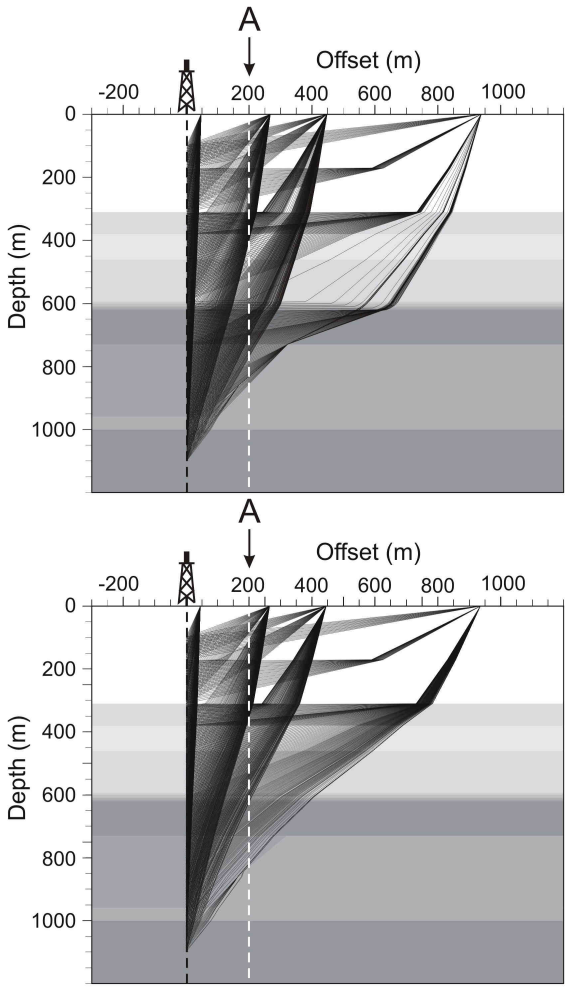

Figure 12: Ray paths for direct P (top panel) ad transmitted converted PS arrivals at the limestone interfaces in the model of Fig. 8 (bottom panel).

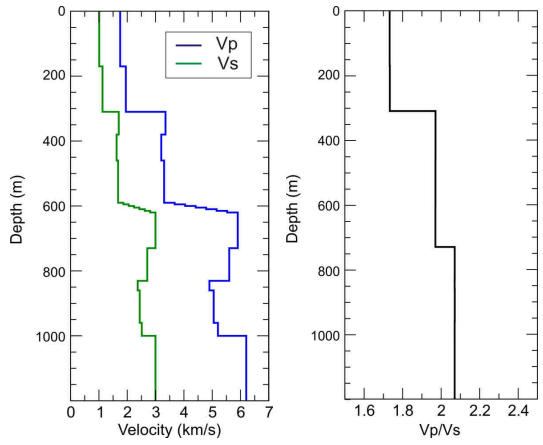

Figure 13: Velocity profiles at 200 m offset, shown by the arrow A in the models of Fig. 12.

Figure 14 shows the result of the multioffset signal processing, compared and superimposed to the surface seismic section G13 (Della Vedova et al., 2013) passing through the well, time migrated data. The VSP signal improves the identification and resolution of the local structures near the well and characterizes dipping events interpretable in the seismic section. In Fig. 15 we see the multi-offset CDP transform represented in depth, with the interpretation of the structural features in the reservoir at the well location, compared to the Vp/Vs ratio estimated at 200 m offset from the well.

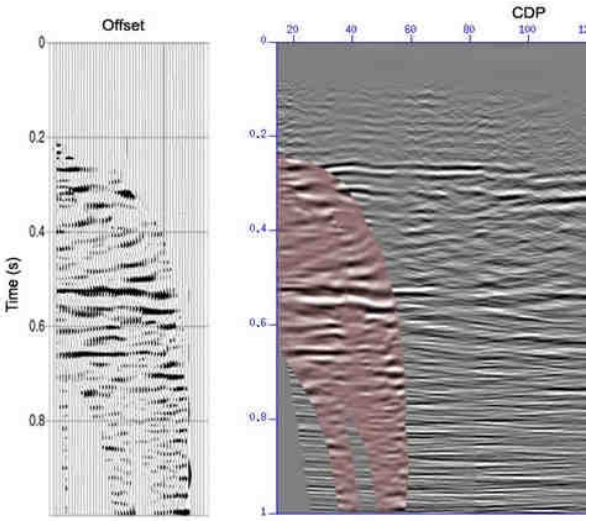

Figure 14: Multi offset VSP time section, compared (left) and superimposed (right side) to the seismic line G13 passing through the well.

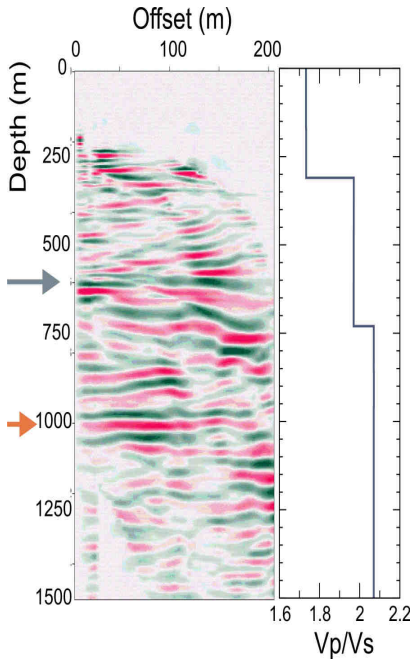

Figure 15: Multi-offset VSP depth section, showing structural features in the proximity of the well, with the interpretation of main changes in the carbonate platform. The grey arrow indicates the top of the Paleogene, the orange arrow indicates the top of the Mesozoic carbo-natic platforms. The right panel shows the Vp/Vs curve calculated at 200 m offset.

5. CONCLUSIONS

The analysis of the full waveform offset signals and of viscoelastic synthetic signals (including anisotropy), integrated with lateral seismic imaging, improved the characterization of the geothermal reservoir coherent with the available geological and geophysical data.

The results include the recognition of changes in the elastic rock properties within the reservoir formations obtained using the converted components to estimate the VP/VS ratio. The results (Figs. 8, 14 and 15) suggest significant lateral changes both in the over-burden terrigenous formations and in the carbonatic geothermal reservoir, as expected at the active Dinaric deformation front. The Grado-1 well is located on the frontal Dinaric thrust likely interested by strike-slip transfer faults with anti-Dinaric direction (NE-SW), as suggested by the regional tectonic reconstruction (Cimolino et al., 2010) and by the companion seismic and gravity investigations (Della Vedova et al., 2013). This network of fractures and the associated deformation was locally imaged to the east of Grado-1 well by borehole seismic investigations.

REFERENCES

Blias, E.: Accurate interval Q-factor estimation from VSP data, *Geophysics*, **77** (3), (2012), WA149–WA156.

Cimolino, A., Della Vedova, B., Nicolich, R., Barison, E. and Brancatelli G.: New evidence of the outer Dinaric deformation front in the Grado area (NE-Italy), *Rendiconti Lincei*, **21**, Supplement 1, (2010), 167–179.

Della Vedova, B., Petronio, L., Poletto, F., Palmieri, F. and Marcon, A.: Reservoir characterization for the completion of the geothermal district heating system in Grado (NE Italy), *Proceedings of the European Geothermal Congress 2013*, Pisa, Italy, (2013), *in press*.

Eberhart-Philips, D., Stanley, W. D., Rodriguez, B. D. and Lutter, W. J.: Surface seismic and electrical methods to detect fluids related to faulting, *Journal of Geophysical Research*, **100**, no. B7, (1995), 12919–12936.

Hauge, P. S.: Measurements of attenuation from vertical seismic profiles, *Geophysics*, **46** (11), (1981), 1548–1558.

Petronio, L., Poletto, F., Palmieri, F. and Della Vedova, B.: Geophysical investigations of the Grado deep structures (NE Italy) for the location of the second geothermal borehole, *G.N.G.T.S. 31° Convegno Nazionale*, Sessione 3.1, (2012), 28–33.

Sun, F. L., Milkereit, B. and Schmitt, D. R.: Measuring velocity dispersion and attenuation in the exploration seismic frequency band, *Geophysics*, **74** (2), (2009), WA113–WA122.

Thomsen, L.: Weak elastic anisotropy, *Geophysics*, **51** (10), 1954-1966, (1986).

Acknowledgements

Authors thank the Comune di Grado (Italy) for the field support and for the permission to present the results, Gualtiero Böhm for his help in the preparation of ray tracing and modelling results, and Giorgia Pinna for the calculation of the attenuation by log data and VSP.